Use of 10Be to predict atmospheric 14C variations during the laschamp excursion: High sensitivity to cosmogenic isotope production calculations

Alexandre Cauquoin, G. Raisbeck, Jean Jouzel, D. Paillard

USE OF ^{10}Be TO PREDICT ATMOSPHERIC ^{14}C VARIATIONS DURING THE LASCHAMP EXCURSION: HIGH SENSITIVITY TO COSMOGENIC ISOTOPE PRODUCTION CALCULATIONS

Alexandre Cauquoin[1,2] • Grant Raisbeck[1,3] • Jean Jouzel[1] • Didier Paillard[1]

ABSTRACT. The Laschamp excursion is a period of reduced geomagnetic field intensity occurring 40.7 ± 1.0 kyr ago. As a consequence, cosmogenic isotope production increased dramatically and its sensitivity to solar activity was enhanced during this period. The latter occurs because a larger fraction of the lower-energy interstellar galactic cosmic-ray particles, normally excluded by the geomagnetic field, is able to reach Earth's atmosphere. This produces a cosmogenic isotope production sig-nal with a significant structure. As high-resolution ^{10}Be profiles from both Antarctica (EDC) and Greenland (NGRIP–GRIP) during this crucial period are now available, one can use them as input into a box carbon cycle model in order to predict at-mospheric ^{14}C variations due to the Laschamp excursion. For this purpose, ^{10}Be data are converted into ^{14}C, using production calculations for the ^{10}Be-^{14}C conversion, after correction for the estimated difference of sensitivity between polar and global ^{10}Be deposition. Several scenarios of carbon cycle state are simulated, from preindustrial to glacial conditions. Applying two recent cosmogenic isotope production calculations for the ^{10}Be to ^{14}C conversion, we found that the resulting atmospheric Δ^{14}C variations are very sensitive to which of these two are employed. For example, Δ^{14}C amplitude under glacial conditions varies from 260‰ (EDC) and 320‰ (Greenland) to 430‰ (EDC) and 510‰ (Greenland) depending on the formulation used for ^{10}Be-^{14}C conversion.

1. INTRODUCTION

Cosmogenic isotopes like ^{14}C and ^{10}Be are produced in Earth's atmosphere mainly by interaction of galactic cosmic rays (GCR) with nitrogen of the upper atmosphere. Since the GCR flux is modulated by the geomagnetic and heliomagnetic fields, records of ^{14}C and ^{10}Be provide useful information about variations in solar activity and geomagnetic field intensity in the past (Lal and Peters 1967). As a consequence, the higher the solar or geomagnetic field, the more primary cosmic-ray particles are deflected, which leads to a decrease of cosmogenic isotope production.

^{14}C and ^{10}Be have been studied in natural archives for several decades. ^{14}C measurements were performed to establish ^{14}C calibration records because the ratio ^{14}C/^{12}C in the atmosphere has changed during the past due to variations in production (geomagnetic field intensity and solar activity) and modifications of the carbon cycle. Many such studies have been done in sediments (Hughen et al. 2004, 2006; Bronk Ramsey et al. 2012), speleothems (Beck et al. 2001; Hoffmann et al. 2010), corals (Fairbanks et al. 2005), and tree rings (Muscheler et al. 2008; Turney et al. 2010). Calibration curves, regrouping all ^{14}C measurements, as IntCal04 and IntCal09 (Reimer et al. 2004, 2009), have been constructed for the conversion of ^{14}C ages to calibrated ages. ^{10}Be has been studied in ice cores from Antarctica (Yiou et al. 1985; Raisbeck et al. 1990, 1992; Horiuchi et al. 2008; Baroni et al. 2011) and Greenland (Beer et al. 1990; Finkel and Nishiizumi 1997; Yiou et al. 1997; Wagner et al. 2001; Muscheler et al. 2004, 2005), as well as in sediments (Raisbeck et al. 1985; Robinson et al. 1995; Frank et al. 1997; Ménabréaz et al. 2011; Nilsson et al. 2011). One advantage of ice cores is that they offer a relatively simple way to calculate ^{10}Be fluxes (from the measured concentration of ^{10}Be and the estimated accumulation rate). Moreover, their higher resolution can be helpful for the study of shorter events due to solar activity, for example.

Although ^{14}C and ^{10}Be are both produced by cosmic rays, their behaviors differ in the atmosphere. Indeed, ^{10}Be atoms become fixed to aerosols and are deposited very quickly after their production

1. Laboratoire du Climat et de l'Environnement/Institut Pierre Simon Laplace (LSCE/IPSL CEA-CNRS-UVSQ), Orme des Merisiers, CEA Saclay, 91191 Gif-sur-Yvette, France.
2. Corresponding author. Email: Alexandre.Cauquoin@lmd.jussieu.fr. Present adress: Laboratoire de Météorologie Dynamique (LMD), Université Paris 6, Tour 45-55, 75252 Paris Cedex 05, France.
3. Centre de Sciences Nucléaires et de Sciences de la Matière (CSNSM), UMR CNRS 8609, Université Paris-Sud XI, Bât 108, 91405 Orsay, France.

(within ~1–2 yr according to Raisbeck et al. [1981]), whereas the ^{14}C atom is oxidized to CO_2 and enters the global carbon cycle, in which it is homogenized with stable carbon. As a consequence, ^{14}C concentration variations in different reservoirs are smoothed and delayed with respect to ^{14}C produc-tion variations. Masarik and Beer (1999) found that the stratosphere contributes 56% of the global production of ^{10}Be and Heikkilä et al. (2009) determined with their model that the stratospheric fraction of the total production is 65%. While most ^{10}Be produced in the troposphere is deposited near the latitude band in which it is formed, even the dominant proportion coming from the strato-sphere probably does not have the time to be completely well mixed because of its relatively short residence time compared to the mixing time of the air in the stratosphere. According to Field et al. (2006), the polar flux is about 20% less sensitive to variations of geomagnetic field intensity (and 20% more sensitive to variations of solar activity) than the global production. This fact will be taken into account for the ^{10}Be-^{14}C conversion (see section 2.2).

The past ^{14}C production rate has been previously studied using numerical models. Past changes of atmospheric ^{14}C concentration were, in most cases, simulated using geomagnetic intensity re-cords retrieved from oceanic sediments (like NAPIS-75 [Laj et al. 2002] or GLOPIS-75 [Laj et al. 2004]). The geomagnetic intensity signal was converted into ^{14}C production with the help of calcu-lations from Masarik and Beer (1999) (equations in Wagner et al. 2000). These model results can be compared with reconstructed $\Delta^{14}C$ values obtained from well-dated archives like sediment records (Hughen et al. 2004, 2006) or speleothems (Beck et al. 2001; Hoffmann et al. 2010). Recently, Hoffmann et al. (2010) used this method with GLOPIS-75 but converting it with an approximation from Elssasser et al. (1956) (see section 2.3) instead of the numerical values from Masarik and Beer (1999). We will show here that the choice of production calculations can have huge consequences on the simulated atmospheric $\Delta^{14}C$. As for ^{10}Be records, Bard et al. (1997), using the same approach as Beer et al. (1988), compared ^{10}Be-based ^{14}C (modeled from the South Pole record of Raisbeck et al. [1990]) with tree-ring ^{14}C records to document how solar modulation has influenced the cosmo-nuclide production variations during the last millennium. Muscheler et al. (2004) used a model with a ^{10}Be composite record from GRIP and GISP2 (Greenland) as an input to compare it with $\Delta^{14}C$ from different sources, especially during the last 25 kyr. Nilsson et al. (2011) also studied atmospheric $\Delta^{14}C$ adopting the same model but with the ^{10}Be GRIP record on the GICC05 timescale between 50 and 25 kyr BP.

Hereafter, we focus on the period around the Laschamp excursion. There has been considerable discussion about the magnitude and origin of high-level atmospheric $\Delta^{14}C$ measured in different archives at the time of this event. The Laschamp excursion represents a well-constrained geochro-nological event and has been dated at 40.7 ± 1.0 kyr ago by Singer et al. (2009). During this event, the geomagnetic field intensity was extremely weak (around 10% of present intensity). This had the effect to sharply increase cosmogenic isotope production (such as ^{10}Be and ^{14}C) (Raisbeck et al. 2007). Moreover, cosmogenic isotope production was affected by an increased sensitivity to solar activity during this event. Indeed, a larger fraction of the lower-energy interstellar galactic cosmic ray particles, normally excluded by the geomagnetic field, was able to reach Earth's atmosphere. For example, Wagner et al. (2001) show that a 205-yr cycle, assumed to be of solar origin, was enhanced in the GRIP ^{10}Be record during the Laschamp excursion. High-resolution ^{10}Be profiles, with consid-erable structure, from both Antarctica (EDC, Raisbeck et al. 2007) and Greenland (NGRIP–GRIP, Yiou et al. 1997, Raisbeck et al. 2007, unpublished data) during this period being now available, it was interesting to use them as input in a box carbon cycle model to predict the resulting atmospheric $\Delta^{14}C$ amplitude linked to the Laschamp excursion. For this, ^{10}Be data need to be converted into ^{14}C production. We will show that this step is crucial to determine the amplitude of atmospheric $\Delta^{14}C$ during this time. Indeed, new calculations of ^{14}C production from Kovaltsov et al. (2012) combined

with those from Kovaltsov and Usoskin (2010) for ^{10}Be production calculations lead to a discrepan-cy in the resulting atmospheric Δ^{14}C amplitude for low geomagnetic field intensity (as the Laschamp excursion) compared with those of Masarik and Beer (2009) (see sections 2.2 and 4.1).

2. MODELING

2.1. ^{10}Be Records from Greenland and EPICA Dome C

Three records were used for this analysis: one from the Antarctic plateau and two from Greenland, plus the geomagnetic field intensity GLOPIS-75 record (see section 2.3). One of the advantages of using ^{10}Be from ice cores is the high resolution, which permits to take into account the structure of the cosmogenic production peak due to increased sensitivity to solar activity. The Antarctic record is EPICA Dome C (Raisbeck et al. 2007) and its time resolution is ~10 yr between the 37.5 and 45.5 kyr BP age range. EDC (75°06′S, 123°21′E) has been synchronized (Raisbeck et al., unpublished data) to the North GRIP (NGRIP) timescale GICC05 (Svensson et al. 2008) between 40.4 and 42.1 kyr BP using the Match protocol from Lisiecki and Lisiecki (2002). The NGRIP record (75.1°N, 42.3°W) has an average time resolution of ~7 yr in the time range 40,424–42,040 yr BP. In order to have a more extended (37.5–45.5 kyr BP) Greenland input for the model, we complement-ed the NGRIP record with the GRIP record (72.5°N, 37.3°W), which has a time resolution from ~30–50 yr (Yiou et al. 1997; Raisbeck et al. 2007), for the rest of the timescale. The two Greenland ice-core records were placed on the GICC05 timescale (Svensson et al. 2008) and were normalized to the same average value over their common age range. To study production variations in ice cores, especially during periods of variable climate, it is probably better to use ^{10}Be flux instead of concentrations because ^{10}Be concentration is influenced not only by production variations but also by the amount of precipitation at the site. Assuming that ^{10}Be falls mainly by dry deposition on the Antarctic plateau (Yiou et al. 1985; Raisbeck et al. 1992), we can minimize the climatic component (precipitation) of the EDC record by calculating ^{10}Be flux, which is the product of the measured concentrations and the estimated accumulation rates (Raisbeck et al. 1992). The ^{10}Be GRIP flux was calculated using the ss09sea accumulation rate (Johnsen et al. 2001). The Greenland and EDC records are reported in Figures 1b and 1c, respectively. The GLOPIS-75 record (Laj et al. 2004) is also displayed for comparison in Figure 1a. The high-pass filtered ^{10}Be flux of each record (cut-off frequency = 1/2000 yr^{-1}), representing variations of production dominated by solar activity, is shown in Figures 1d and 1e.

The EDC and Greenland records are different in several aspects. For EDC, the assumption that ^{10}Be falls by dry deposition is probably reasonable because this is a very dry region with an extremely low and relatively stable accumulation rate (EPICA 2004). Greenland is not as dry as the Antarctic plateau and the snow accumulation rate is more variable. It is important to keep in mind that cal-culated ^{10}Be fluxes are directly affected by uncertainties in the estimated accumulation rate of the studied sites. Moreover, the Greenland record has some additional limitations like the uncertainties about the ^{10}Be GRIP record (resolution, missing samples, corrections for filtered samples, Yiou et al. 1997; Raisbeck et al. 2007), and its combination with NGRIP.

2.2. Reconstruction of ^{14}C Production from ^{10}Be Flux

To calculate the ^{14}C production rate from the ^{10}Be flux, we assume that long-term variations (≥2000 yr) are due to fluctuations of the geomagnetic field intensity and variations on shorter time-scales correspond to changes in solar activity (Muscheler et al. 2005). To make this separation (Fig-ure 1: bold curves), we used the AnalySeries program from Paillard et al. (1996). First, a correction to take into account the latitudinal dependency of ^{10}Be deposition is applied because, contrary to ^{14}C, ^{10}Be is probably not completely homogenized before its deposition in polar regions. Contribu-

tions from different regions to the flux of ^{10}Be deposited in polar regions have been estimated by comparisons of calculated ^{10}Be production from changes in geomagnetic field intensity with ^{10}Be records. Using the Vostok ice core, Mazaud et al. (1994) deduced that 25% of ^{10}Be was locally produced and 75% was modulated by global geomagnetic intensity changes. More recently, by the use of model-derived estimates, Field et al. (2006) found that polar deposition in both hemispheres is enhanced by a factor of 1.2 (compared with global deposition) for solar-activity-induced variations and reduced by a factor of 0.8 for geomagnetic intensity variations. We used these results in order to estimate the global ^{10}Be flux (see section 1). In contrast to Field et al. (2006), Heikkilä et al. (2008), using the ECHAM5-HAM General Circulation Model, found no indication of a polar enhancement. Indeed, they found ^{10}Be "well-mixed" in the stratosphere, which is sufficient to mask a latitudinal dependence in the polar regions (Heikkilä et al. 2009). Muscheler et al. (2004) and Nilsson et al. (2011) assumed that the ^{10}Be flux from Greenland they used for Δ^{14}C modeling was an indicator of changes in global ^{10}Be production. Using this last hypothesis for our input and our carbon cycle model would decrease the atmospheric Δ^{14}C amplitude modeled by 30–60‰ depending on the ^{10}Be-^{14}C conversion used (see chapter below and section 4.1).

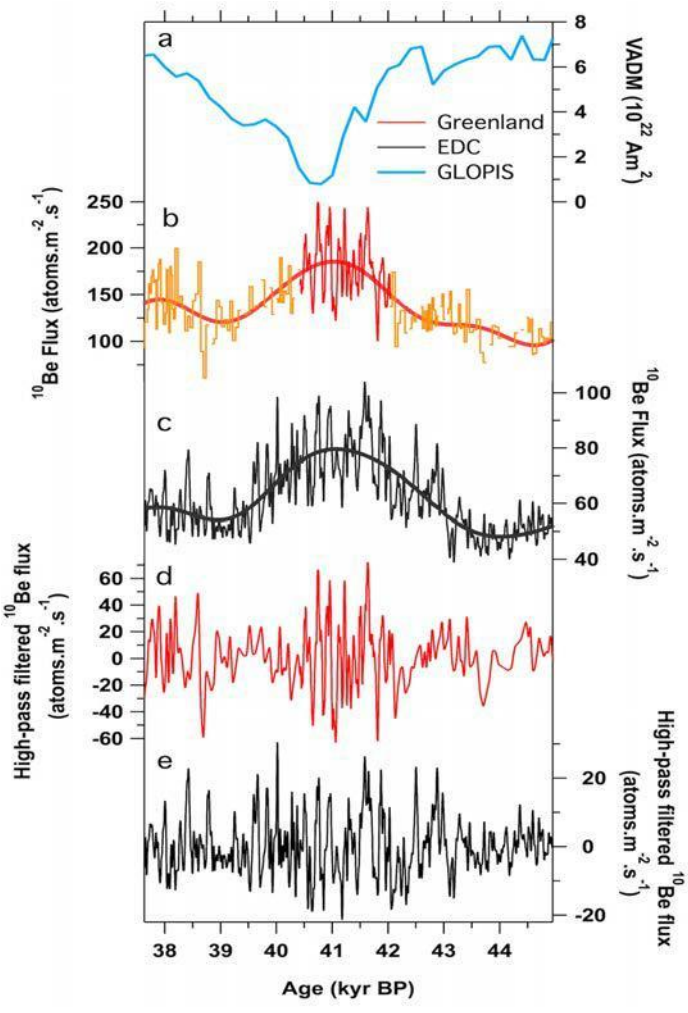

Figure 1 (a) GLOPIS-75 record (Laj et al. 2004). (b, c) ^{10}Be flux measured in the Greenland (red) and EDC (black) ice cores between 37.5 and 45.5 kyr BP. EDC has been synchronized with NGRIP between 40 and 42 kyr BP on the GICC05 age scale. The Greenland record is a combination of NGRIP (thin red line) and GRIP (orange) data. The NGRIP record covers the time range 40,424–42,040 yr BP while the GRIP data are used over the rest of the timescale. The GRIP data were scaled in such a way that GRIP and NGRIP fluxes have the same average value over their common age range. The bold curves show the data after low-pass filtering (cutoff frequency = 1/2000 yr^{-1}) assumed to be the geomagnetic component. (d, e) ^{10}Be flux in the Greenland (red) and EDC (black) ice cores after removing the low-pass component given by the bold curves in (b) and (c), describing fast variations of ^{10}Be probably dominated by solar activity variations.

After applying these corrections to ^{10}Be, we account for difference in production processes between ^{10}Be and ^{14}C. ^{14}C is produced by absorption of thermal neutrons while ^{10}Be is produced by spallation reaction (mainly with high-energy neutrons) (Masarik and Beer 1999, 2009). Expressions in the article of Wagner et al. (2000) (using the results of Masarik and Beer [1999]) were previously used by Muscheler et al. (2004) and Nilsson et al. (2011) for ^{10}Be-^{14}C conversion, and also by others (Laj et al. 2002; Hughen et al. 2004, 2006) to calculate the ^{14}C production rate from geomagnetic intensity record (see section 1). An update of these calculations has been released by Masarik and Beer (2009). To our knowledge, it has not yet been applied for this type of study. Very recently, Kovaltsov et al. (2012) simulated ^{14}C production after having calculated ^{10}Be production variations according to geomagnetic field intensity and solar activity (Kovaltsov and Usoskin 2010). For con-venience, the ^{10}Be-^{14}C calculations of Kovaltsov and Usoskin (2010) and Kovaltsov et al. (2012) will be called KOV. Results of these two sets of calculations are shown as a function of the geo-magnetic field intensity (B, relative to the present value) in Figure 2. As can be seen, the predictions of relative ^{10}Be at low geomagnetic intensity, as well as the slope of the ^{14}C/^{10}Be production ratio as a function of the geomagnetic field intensity are very different for these two theoretical models. This has great consequences on the resulting atmospheric Δ^{14}C amplitude due to weak geomagnetic shielding during the Laschamp excursion (see section 4.1). Assuming that solar activity was on average constant during the studied period (solar modulation potential ϕ = 550 MV according to the definition of Castagnoli and Lal 1980), the sensitivity difference of ^{10}Be and ^{14}C to solar activ-ity as a function of geomagnetic field intensity is also taken into account for shorter-term changes (<2000 yr). The difference in the definition of the local interstellar spectrum (LIS) used by Masarik and Beer (2009) and KOV (Kovaltsov and Usoskin 2010; Kovaltsov et al. 2012) is taken into ac-count using the relation in the appendix of Usoskin et al. (2005). We have also shown in Figure 2a the approximation from Elsasser et al. (1956) used by Hoffmann et al. (2010) to convert the GLO-PIS-75 geomagnetic intensity record (Laj et al. 2004) into ^{14}C production. The consequences of the choice of Hoffmann et al. (2010) on simulated atmospheric Δ^{14}C is discussed below in section 2.3.

2.3. Approximation of Hoffmann et al. (2010)

Hoffmann et al. (2010) simulated atmospheric Δ^{14}C from 45 to 28 kyr BP with the GLOPIS-75 geomagnetic intensity record (Laj et al. 2004) as input and found an amplitude of 550‰ which is consistent with their ^{14}C measurements from a speleothem. This type of simulation has been previ-ously done by Laj et al. (2002) or Hughen et al. (2004, 2006) with more simple carbon cycle mod-els. Unlike Hoffmann et al. (2010), they did not find such a large amplitude. The major difference between the simulation of Hoffmann et al. (2010) and the others is not so much the complexity of the carbon cycle model employed, but the use of the following approximation

$$P/P_0 = \sqrt{\frac{1}{M/M_0}}$$

from Elsasser et al. (1956) (with P the time-varying ^{14}C production rate, P_0 the present-day produc-tion rate, M the time-varying global geomagnetic intensity, and M_0 the present geomagnetic intensi-ty) instead of the relationship of Wagner et al. (2000) or Masarik and Beer (2009) (e.g. Figure 2a) for the production input. To illustrate this point, we show in Figure 3 how the GLOPIS-75 geomag-netic intensity record is converted into relative global ^{14}C production rate using either the Masarik and Beer (2009) values (red), the KOV calculations (in green; Kovaltsov et al. 2012), or the Hoff-mann et al. (2010) approximation (black). The impact of this approximation can be seen when the geomagnetic field intensity is low (curve b in Figure 3). Indeed, the maximum ^{14}C production rate rises by factors of 2.13 and 2.08 with the Masarik and Beer (2009) and Kovaltsov et al. (2012) for-

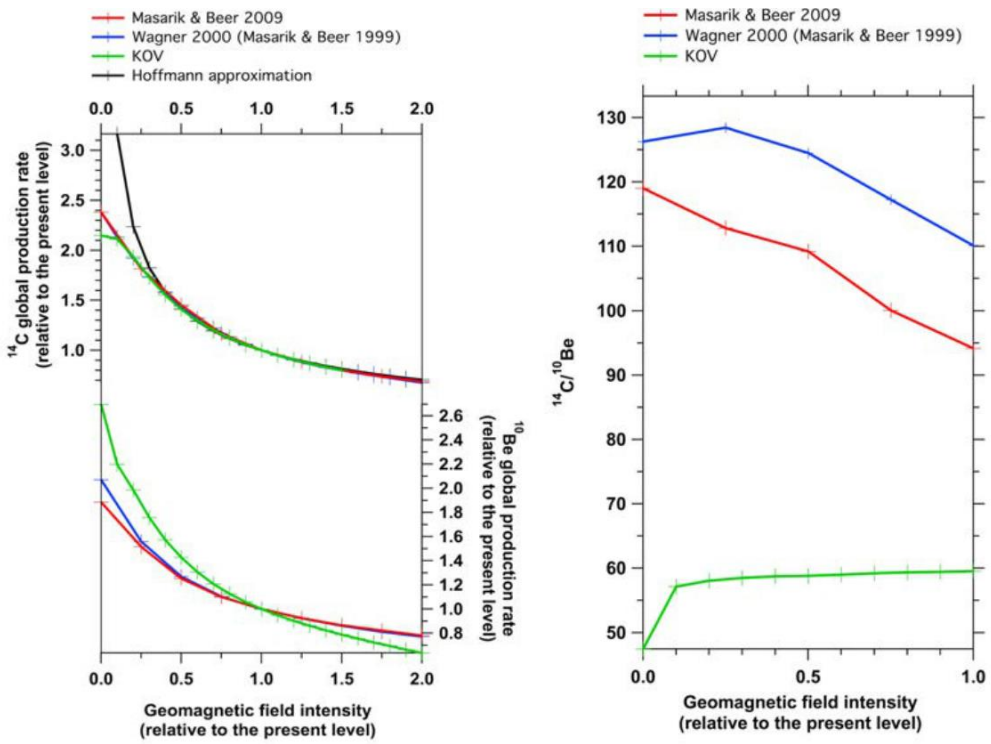

Figure 2 (a) Dependence of predicted relative ^{14}C and ^{10}Be global production rate on geomagnetic field intensity for the solar modulation parameter ϕ = 550 MV (based on the definition of Castagnoli and Lal 1980). The blue curves are the production rates according to Wagner et al. (2000) (Masarik and Beer 1999), the red curves represent the update from Masarik and Beer (2009), and the green curves come from the calculations of Kovaltsov and Usoskin (2010) for ^{10}Be and Kovaltsov et al. (2012) for ^{14}C. The black curve of ^{14}C global production rate corresponds to the approximation used by Hoffmann et al. (2010). (b) ^{14}C/^{10}Be production rate ratio as a function of geomagnetic field intensity according to Masarik and Beer (1999) (blue), Masarik and Beer (2009) (red), and the KOV simulation (Kovaltsov and Usoskin 2010; Kovaltsov et al. 2012, green).

mulas, respectively, while it increases by a factor of 3.16 with the approximation. Indeed, because the geomagnetic intensity was less than 20% of its present value during the Laschamp excursion, the use of this approximation for this period (Hoffmann et al. 2010) is not appropriate. We can conclude that this approximation has a large effect of amplification on the ^{14}C production rate signal, and thus on the simulated atmospheric Δ_{14}C.

We used the three production-rate curves shown in Figure 3 as input to the carbon cycle model (presented in section 2.4) in order to see the consequences on modeled atmospheric Δ_{14}C (bottom of Figure 3). The difference between the formula employed by Hoffmann et al. (2010) and the others is large: around 150‰ compared to Masarik and Beer (2009) or Kovaltsov et al. (2012) formula-tions. This means that the 550‰ amplitude found by Hoffmann et al. (2010) is partly an artifact due to this approximation, showing the importance of the formulas used to make the conversion from geomagnetic intensity into global ^{14}C production rate. In comparison, previous simulations made by Laj et al. (2002) or Hughen et al. (2004, 2006), who worked with geomagnetic records, and the Masarik and Beer (1999) conversion (very similar to Masarik and Beer (2009) for ^{14}C production, e.g. Figure 2a) as input of their model, found an amplitude of ~300‰ and >200‰, respectively for preindustrial conditions (see section 2.5). This is in good agreement with the amplitude of 290‰ simulated with our carbon cycle model using GLOPIS-75 and the equation from Masarik and Beer

(2009) (see red curve, Figure 3c), showing that our carbon cycle model gives results coherent with previous studies. We note that these results using Masarik and Beer (2009) and KOV calculations are smaller than the $\Delta_{14}C$ amplitude from IntCal09 of Reimer et al. (2009) (e.g. Figure 7, >450‰).

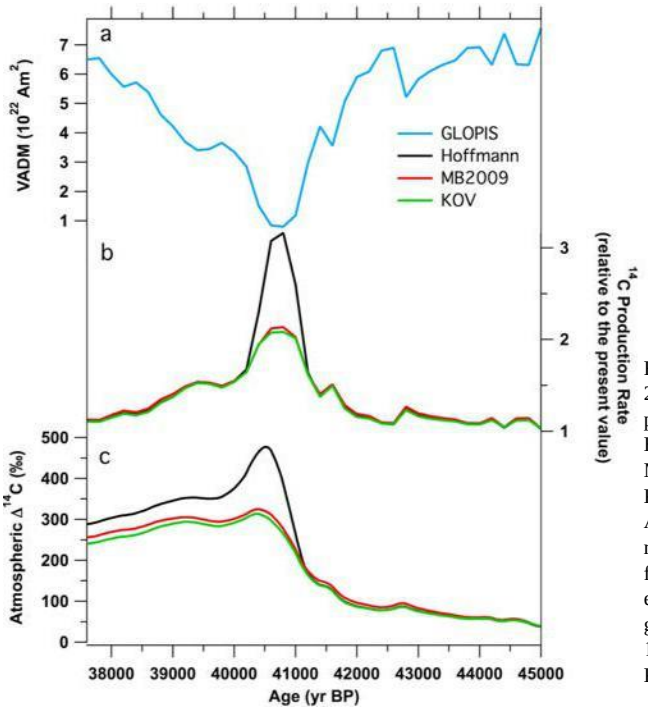

Figure 3 (a) GLOPIS-75 record (Laj et al. 2004). (b) Comparison between converted ^{14}C production from GLOPIS-75 record with the Hoffmann et al. (2010) approximation (black), Masarik and Beer (2009) update (red), and Kovaltsov et al. (2012) simulation (green). (c) Atmospheric $\Delta_{14}C$ obtained from production records in (b) with the 12-box model. The differences in amplitude between the Hoffmann et al. (2010) approximation and the different global ^{14}C production calculations are around 150‰ with the Masarik and Beer (2009) and Kovaltsov et al. (2012) formulations.

In addition to the reasons discussed in section 1, the use of ^{10}Be flux records in ice cores has two advantages compared to geomagnetic intensity record in sedimentary cores: they have a higher resolution allowing the study of solar activity, and there is expected to be less uncertainty in the ice accumulation rate compared to that of sediments, and thus a more reliable chronology for duration of short-term events such as the Laschamp excursion.

2.4. Description of the Carbon Cycle Model

To investigate the influence of the Laschamp event on atmospheric $\Delta_{14}C$, we used a 10-box ocean model (plus an atmosphere box and biosphere box) made with the BoxKit2 program (Paillard 1995) to simulate the carbon cycle (Figure 4). This program was already used by Laj et al. (2002) for their model with 17 boxes but no biosphere. The advantage of BoxKit2 is its flexibility: it is easy to vary the volume and areas of boxes, or the values of fluxes. To build our carbon cycle model, we were inspired by PANDORA (Broecker and Peng 1986) and other models (Siegenthaler et al. 1980; Bard et al. 1997; Laj et al. 2002; Hughen et al. 2004). There exist several results of global average produc-tion rate for ^{10}Be and ^{14}C at present conditions (Webber and Higbie [2003]; Kovaltsov and Usoskin [2010] for ^{10}Be; Kovaltsov et al. [2012] for ^{14}C; Masarik and Beer [1999, 2009] for both cosmogenic isotopes). Because our carbon cycle model is similar to Bard et al. (1997), we have adopted the same global ^{14}C production rate value (1.72 at m^{-2} s^{-1}). Our model was then used to simulate atmospheric $\Delta_{14}C$ changes in response to changing ^{14}C production during the Laschamp event. We focus on the period between 45,500 and 37,500 yr BP. A figure with the values of fluxes as well as a table with box volumes and areas are given in the Supplementary Material accompanying the online version of this article (https://journals.uair.arizona.edu/index.php/radiocarbon/article/view/16478).

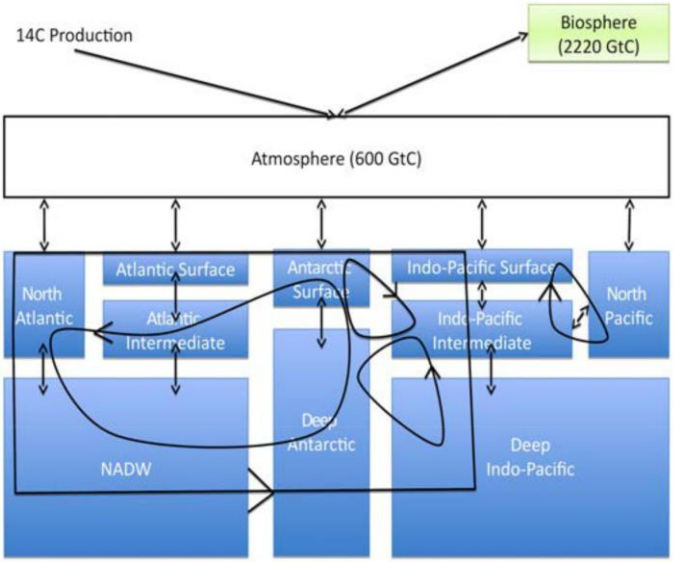

Figure 4 Scheme representing our 12-box model (10 ocean boxes + 1 atmo-sphere and biosphere box).

To examine if our model is coherent with previous studies, we first tested the damping and phasing effect of the model, depending on the frequency of production variations, as shown in Figure 5. For this, we have used sinusoidal changes of cosmogenic production as a model input. The frequencies used run from 5 to 10_5 yr. The attenuation effect is such that variations in $_{14}$C production are attenu-ated by a factor of ~100 for decadal cycles, ~20 for centennial scales, and ~10 for millennial cycles (see top of Figure 5). This is coherent with other models (Delaygue and Bard 2011). Note that the atmosphere in the model is well mixed, without separation of the troposphere and the stratosphere, which affects the results for periods under 30 yr (Siegenthaler et al. 1980). The other effect of the carbon cycle is the delay between atmospheric $_{14}$C concentration and variations in production, expressed as a phase lag in Figure 5. For example, century-scale periodicities are shifted by a few decades (bottom of Figure 5). The phase lag of the model is coherent with values presented in De-laygue and Bard (2011).

2.5. Simulations of the Carbon Cycle

With this model, it is possible to have an idea of the impact of the geomagnetic and solar modula-tions on atmospheric $_{14}$C/C. It is interesting to examine effects of changes in the carbon cycle too, because the Laschamp excursion occurred during a glacial period but straddled the DO-10 (Dans-gaard-Oeschger) interstadial. Several simulations were made with different carbon cycle boundary conditions. The first one (which we call S1) corresponds to the modern preindustrial boundary conditions (light colored curves in Figure 6). The simulation S2 is similar but with the atmosphere and terrestrial biosphere reduced to, respectively, 75% and 65% of their preindustrial carbon inven-tories (Indermühle et al. 2000; Hughen et al. 2004). The results of this simulation are plain colored in Figure 6. For the third simulation (S3), we added a reduction of the North Atlantic Deep Water (NADW) fluxes by one-third (Laj et al. 2002; Hughen et al. 2004) to simulate estimated glacial conditions (dark colored curves in Figure 6). The system is initialized at an equilibrium state before the beginning of the simulation.

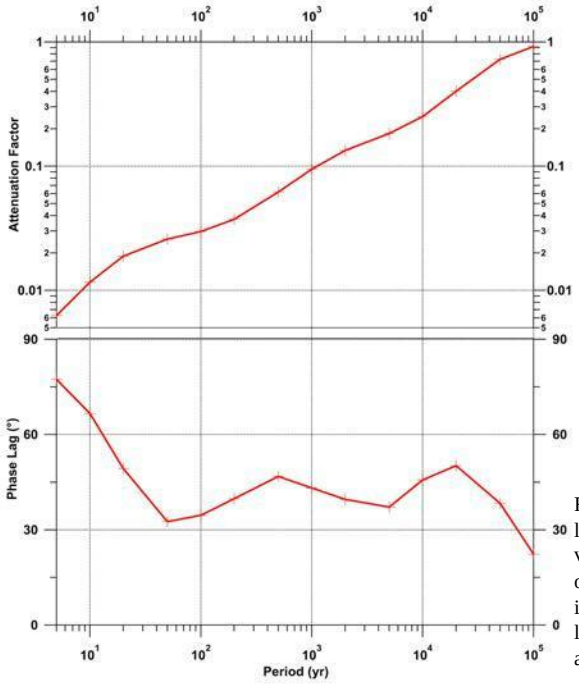

Figure 5 Simulated attenuation factor (top) and phase lag (bottom) of atmospheric ratio $^{14}C/C$ for sinusoidal variations in ^{14}C production, as a function of the period of these variations. The attenuation factor is normalized to the size of the production change. The phase lag is calculated as the time lag divided by the period and multiplied by 360°.

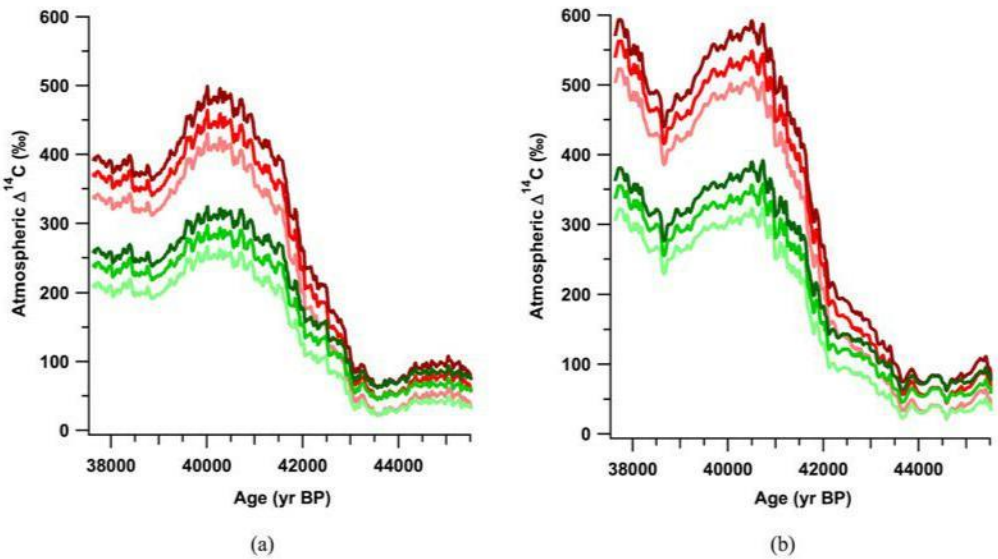

Figure 6 Relative variations in atmospheric ^{14}C content simulated by applying the ^{10}Be-based ^{14}C production for (a) EPICA Dome C (Antarctica) and (b) Greenland. Light curves correspond to preindustrial conditions (S1), plain curves to reduced carbon inventories of atmosphere and biosphere (S2), and dark curves to glacial conditions (S3 = S2 + re-duction of NADW formation). Red and green curves represent atmospheric $\Delta^{14}C$ variations using ^{10}Be-^{14}C conversion from Masarik and Beer (2009) and KOV (Kovaltsov and Usoskin 2010; Kovaltsov et al. 2012), respectively.

3. RESULTS FROM ^{10}Be FLUX RECORDS

Here, we discuss $\Delta^{14}C$ variations inferred from the ^{10}Be-based production rate, using calculations from Masarik and Beer (2009) and the KOV simulation (Kovaltsov and Usoskin 2010; Kovaltsov

et al. 2012), with the different scenarios presented in section 2.5. The results are presented in section 3.1 for EPICA Dome C (Antarctica) and in section 3.2 for the composite ^{10}Be record from Greenland. All graphs are brought together in Figure 6. The results using Masarik and Beer (2009) formulas and KOV calculations are in red and green, respectively. Moreover, we compare our results from assumed glacial conditions (S3) with Δ^{14}C from IntCal09 calibration curve in section 3.3 (Reimer et al. 2009).

3.1. EPICA Dome C

The resulting Δ^{14}C from the EDC input with the calculations of Masarik and Beer (2009) and KOV (Kovaltsov and Usoskin 2010; Kovaltsov et al. 2012) are shown in Figure 6a under the different scenarios. Concerning the results using Masarik and Beer (2009), atmospheric Δ^{14}C increases by 400‰ using the modern case simulation S1 (light red). Applying simulations S2 and S3 (plain and dark red curves, see section 2.5) gives relatively minor changes on atmospheric Δ^{14}C (amplitude of 410‰ with simulation S2 and 430‰ with simulation S3). Using KOV calculations, we obtain am-plitudes of 235‰, 250‰, and 260‰ with scenarios S1, S2, and S3, respectively. We can see that the difference in sensitivity between the simulations of ^{10}Be and ^{14}C production (see Figure 2; Masarik and Beer 2009; Kovaltsov and Usoskin 2010; Kovaltsov et al. 2012) leads to very different results in the modeled atmospheric Δ^{14}C from ^{10}Be records (see section 4.1). By contrast, the changes due to the choice of parameters of the carbon cycle model do not seem to influence the results greatly.

3.2. Greenland

The results for the Greenland composite record are presented in Figure 6b. Applying the modern simulation S1 and Masarik and Beer (2009) formulation, the modeled atmospheric Δ^{14}C increases by 475‰. With simulations S2 and S3, atmospheric Δ^{14}C increases only slightly (+10‰ and +35‰ for scenarios S2 and S3, respectively). Using KOV conversion, the variability between the three scenarios is lower with amplitudes of 295‰, 310‰, and 320‰. Note that for the same scenario and calculation, the amplitudes of atmospheric Δ^{14}C obtained with Greenland input are higher than with EDC input.

3.3. Comparison with IntCal09

We compare here our results under assumed glacial conditions (S3) with Δ^{14}C from the IntCal09 calibration curve (Reimer et al. 2009). This comparison is shown in Figure 7. In Figure 7b, simulated Δ^{14}C from ^{10}Be EDC (light) and Greenland (dark) records have been shifted by +195‰ in order to make the initial conditions similar to the IntCal09 curve. As noted before, results of Δ^{14}C using Ma-sarik and Beer (2009) calculations reach a much higher amplitude than those with KOV values. The EDC amplitudes are 430‰ and 260‰ (section 3.1), while the amplitudes of Δ^{14}C with Greenland input are 510‰ and 320‰ (section 3.2) according to the model applied for the conversion. As for Δ^{14}C from the IntCal09 curve, it varies ~400‰ between 37.5 and 45.5 kyr BP (Figure 7b). We con-clude that results using the Masarik and Beer (2009) conversion with ^{10}Be flux seem to be in better agreement with Δ^{14}C amplitude from IntCal09. Δ^{14}C with KOV calculations are much smaller. Sev-eral differences can be seen in comparison to the IntCal09 curve. First, Δ^{14}C from IntCal09 is higher on the absolute scale than the results obtained from ^{10}Be flux (Figure 7a), especially comparing with results using the KOV values. The second peak after the Laschamp excursion (~38.5 kyr BP) on the IntCal09 curve is also present in the Greenland output (but delayed) but not on Δ^{14}C from the EDC record. However, the most dramatic difference between our calculations and IntCal09 is the much steeper increase at the beginning of the Laschamp event. This increase takes ~3000 yr in our cal-culations, and about twice as long in IntCal09. This might be explained by a variable carbon cycle not taken into account in our calculations, or the uncertainties of ^{14}C calibration during this period.

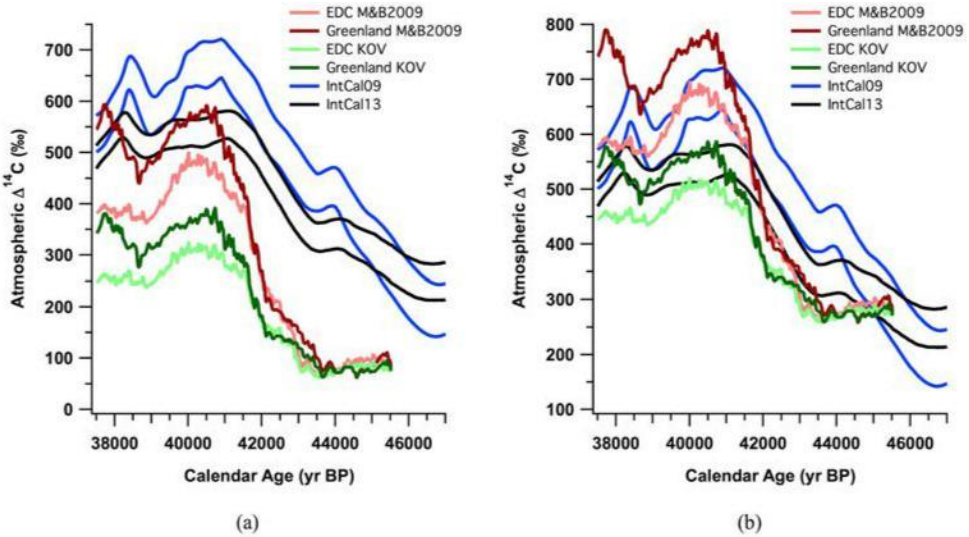

Figure 7 Comparison of $\Delta_{14}C$ from our simulations with scenario S3 with $\Delta_{14}C$ from the IntCal09 and IntCal13 calibration curves (Reimer et al. 2009, 2013). $\Delta_{14}C$ from $_{10}Be$ records are on their absolute scale in (a) and shifted by +195‰ in (b) to focus on the amplitude of the signals. The light and dark curves represent simulated atmospheric $\Delta_{14}C$ using the EDC and Greenland records, respectively. The red and green curves always symbolize $\Delta_{14}C$ varia-tions using $_{10}Be$-$_{14}C$ conversion from Masarik and Beer (2009) and KOV (Kovaltsov and Usoskin 2010; Kovaltsov et al. 2012), respectively. $\Delta_{14}C$ from the IntCal09 and IntCal13 calibration curves (Reimer et al. 2009, 2013) are shown within their 1-standard deviation envelope (blue and black curves, respectively).

4. DISCUSSION

One of the initial motivations of this study was to see whether the increased sensitivity of cosmo-genic isotope production to solar modulation during periods of low geomagnetic intensity could lead to significant fluctuations of $_{14}C$ during the Laschamp event. As can be seen in Figures 6–8 and the simulated calibration curve (Figure S2), while there are fluctuations as large as 30‰, and predicted reversals over a period of several hundred years, these effects are not dramatic. This is due to the strong damping effect of the carbon cycle on centennial production variations.

The results obtained with the help of our simple box model and presented in section 3 confirm sev-eral points: (i) the changes of boundary conditions on the carbon cycle do not significantly influence the resulting amplitudes of $\Delta_{14}C$; (ii) for the same scenario and calculation, the $\Delta_{14}C$ amplitude from EDC is lower than the one from the composite Greenland record (between 60‰ and 80‰ of dif-ference), due perhaps to the aspects discussed in section 2.1; and (iii) the formula used for $_{10}Be$-$_{14}C$ conversion has huge consequences on simulated $\Delta_{14}C$ (see section 4.1). We will thus focus on this last aspect, especially the difference between cosmogenic isotope productions simulated by Masarik and Beer (1999), their update of 2009, and the KOV model (Kovaltsov and Usoskin 2010; Kovaltsov et al. 2012). The possible uncertainties due to carbon cycle changes will also be discussed.

4.1. Sensitivity of $_{10}Be$-$_{14}C$ Conversion

The conversion of $_{10}Be$ (or geomagnetic paleointensity) into $_{14}C$ is certainly the most important point in atmospheric $_{14}C$ modeling (as shown in section 2.3). Different formulations of global $_{10}Be$ and $_{14}C$ production rate as a function of geomagnetic field intensity are presented in Figure 2a. For the geomagnetic intensity B = 0 (and the solar modulation ϕ = 550 MV), global $_{10}Be$ production rates are equal to 2.07, 1.88, and 2.7 (relative to the present level) with the simulation of Masarik and Beer

(1999), their update of 2009, and Kovaltsov and Usoskin (2010) calculations, respectively. KOV calculations show a considerably stronger dependence for ^{10}Be production on the geomagnetic field intensity than Masarik and Beer (1999, 2009). Global ^{14}C production rates reach values of 2.38, 2.38, and 2.2, respectively (Kovaltsov et al. 2012 for the last value). Focusing on the variations of ^{14}C/^{10}Be global production rate ratio as a function of geomagnetic field intensity (Figure 2b), one may notice that (i) the ^{14}C/^{10}Be ratio from KOV (Kovaltsov and Usoskin 2010; Kovaltsov et al. 2012) is clearly lower (by a factor of 2) than the two others (see their respective articles for the absolute value of ^{10}Be and ^{14}C) and (ii) the slopes of ^{14}C/^{10}Be ratios of Masarik and Beer (1999, 2009) and KOV (Kovaltsov and Usoskin 2010; Kovaltsov et al. 2012) calculations are very differ-ent. From B = 1 to B = 0, the ^{14}C/^{10}Be production rate increases by 15% with the Masarik and Beer (1999) simulation, by 26% with their 2009 update, and remains constant with the KOV calculations (Kovaltsov and Usoskin 2010; Kovaltsov et al. 2012), except for $B < 0.1$, where it decreases. This last point has strong consequence on simulated Δ^{14}C, as shown in Figures 6–8. According to J Beer (personal communication), it is the lower-energy threshold for the production of ^{14}C that results in the dependence of the ^{14}C/^{10}Be production ratio with geomagnetic field intensity. This seems intuitively reasonable to us. According to I Usoskin (personal communication), this difference in threshold does not lead to such dependence.

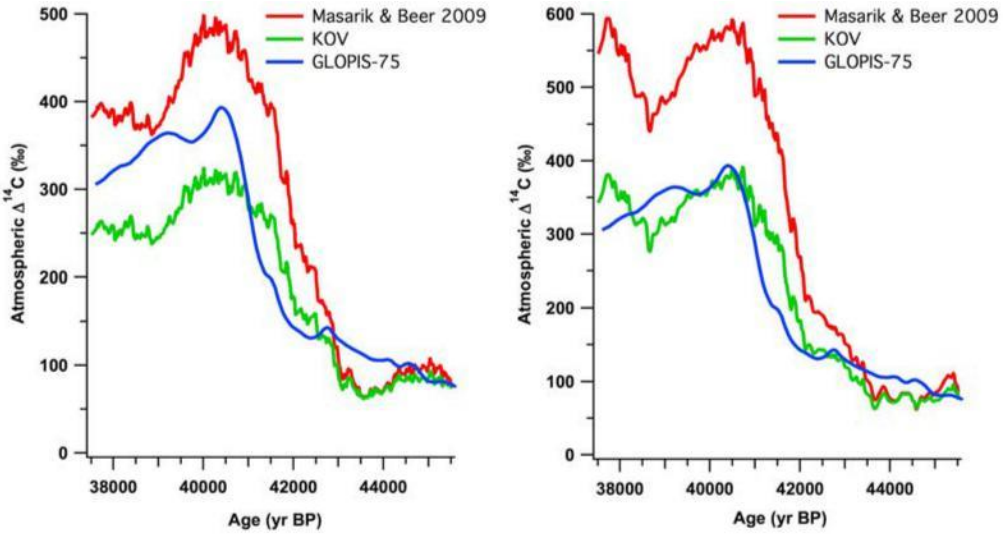

Figure 8 Atmospheric Δ^{14}C simulated under glacial conditions using both production formulations (red: Masarik and Beer 2009; green: Kovaltsov and Usoskin 2010; Kovaltsov et al. 2012) with the EDC (left) and Greenland input (right). Δ^{14}C using GLOPIS-75 (Laj et al. 2004) under glacial conditions is also shown (blue).

Comparing the amplitudes of Δ^{14}C obtained with both calculations (Masarik and Beer [2009], and KOV [Kovaltsov and Usoskin 2010; Kovaltsov et al. 2012]) under glacial conditions (S3), we obtain values of 430‰ and 260‰ for EDC (left graph of Figure 8). For the Greenland input, the resulting amplitudes are 510‰ and 320‰, respectively (right graph of Figure 8). The discrepancy on Δ^{14}C amplitude between the two calculations is huge (approximately a factor of 1.6). We point out that the use of one or the other production calculation for the ^{10}Be-^{14}C conversion leads to a different interpretation of the results during periods of weak geomagnetic shielding. To remedy this situation, it will be necessary to clarify the relative dependence of ^{10}Be production as a function of geomagnetic field intensity.

In contrast to $^{14}C/^{10}Be$, the relative dependence of ^{14}C production on geomagnetic intensity given by Masarik and Beer (2009) and KOV (Kovaltsov et al. 2012) is virtually identical (Figure 2a). This implies that if one assumes the same initial production rate, the two models predict the same ^{14}C response to the Laschamp event, as seen in Figure 3. In Figure 8, we show this response (blue curve) using the same assumed glacial conditions (scenario S3) as used in Figures 6 and 7, and the geomagnetic field intensity given by GLOPIS-75. One can note several differences compared to that found using ^{10}Be. Most obvious is the absence of the fine structure because the geomagnetic field input lacks the solar modulation variations. Also, because the GLOPIS-75 record of the Laschamp event is significantly shorter than that recorded by ^{10}Be (Figure 1), the resulting ^{14}C peak is narrower than that found using ^{10}Be. Finally, as far as amplitude, that found using GLOPIS-75 is midway between the Masarik and Beer (2009) and KOV results using the ^{10}Be input from EDC, while in very good agreement with KOV using ^{10}Be input from Greenland (Figure 8).

4.2. Carbon Cycle Uncertainties

The conversion of ^{10}Be into ^{14}C is not the only uncertainty of the method we have used. Our lack of knowledge about past changes of the carbon cycle brings also some uncertainties. Indeed, because the Laschamp excursion straddles D-O 10 (Yiou et al. 1997; Raisbeck et al. 2007) 41,000 yr ago, the carbon cycle has probably changed during this period, a potential cause of differences between measurements and simulations. For example, in our model it is assumed that oceanic circulation is constant during the experiment between 37.5 and 45.5 kyr BP. In reality, however, rapid varia-tions of temperature happened, as shown by ice-core records (EPICA 2006), probably leading to changes of oceanic circulation and biosphere (and thus carbon cycle). These changes coupled with the Laschamp excursion could modify the $^{14}C/C$ ratio in the atmosphere. Moreover, we began the simulation with a carbon cycle at equilibrium. Depending how the climate (CO_2) changed several thousand years before the period studied, it could influence the resulting atmospheric $\Delta^{14}C$ (release of carbon trapped into deep ocean, for example). An ongoing work with a more sophisticated dy-namical carbon cycle model will focus on the climatic aspects linked to concentration of CO_2 and ocean dynamics.

5. CONCLUSION

Because of their high resolution with a significant structure, ^{10}Be records from EDC and Greenland (GRIP and NGRIP) ice cores are good candidates to study production effects on the amplitude of atmospheric $\Delta^{14}C$ during the Laschamp geomagnetic event. Both production calculations from Ma-sarik and Beer (2009) and KOV (Kovaltsov and Usoskin 2010; Kovaltsov et al. 2012) have been used for the ^{10}Be-^{14}C conversion, leading to discrepant results. Indeed, atmospheric $\Delta^{14}C$ amplitude is different by a factor of 1.6 according to the production calculations applied for the ^{10}Be-^{14}C con-version. Therefore, one must be careful when choosing a production formulation for studying ^{14}C production variations during periods of very low geomagnetic field intensity, such as the Laschamp excursion, using ^{10}Be data. Moreover, we point out the inappropriate use of the approximation from Elsasser et al. (1956) by Hoffmann et al. (2010) for conversion of geomagnetic field intensity into ^{14}C production. It results in a stronger amplitude of atmospheric $\Delta^{14}C$ during periods of weak geo-magnetic shielding (as the Laschamp event) compared to model calculations.

Because of the simultaneity of the Laschamp excursion with D-O event 10 and variations of CO_2 concentration in the atmosphere before the studied period, possible climate effects should be an-alyzed with the help of a dynamical model. Improved understanding of carbon cycle during the glacial period is required, too.

ACKNOWLEDGMENTS

We thank I Usoskin for providing the ^{14}C table before it was published and for his prompt replies to our questions. We thank J Masarik and J Beer for providing numerical values of their calculations and comments regarding their interpretation. We also want to thank C Laj and C Kissel for GLO-PIS-75 data, and E Michel for her useful comments on the model.

REFERENCES

Bard E, Raisbeck GM, Yiou F, Jouzel J. 1997. Solar modulation of cosmogenic nuclide production over the last millennium: comparison between ^{14}C and ^{10}Be records. *Earth and Planetary Science Letters* 150(3–4):453–62.

Baroni M, Bard E, Petit JR, Magand O, Bourlès D. 2011. Volcanic and solar activity, and atmospheric circulation influences on cosmogenic ^{10}Be fallout at Vostok and Concordia (Antarctica) over the last 60 years. *Geochimica et Cosmochimica Acta* 75(22):7132–45.

Beck JW, Richards DA, Edwards RL, Silverman BW, Smart PL, Donahue DJ, Hererra-Osterheld S, Burr GS, Calsoyas L, Jull AJT, Biddulph D. 2001. Ex-tremely large variations of atmospheric ^{14}C con-centration during the last glacial period. *Science* 292(5526):2453–8.

Beer J, Blinov A, Bonani G, Finkel RC, Hofmann HJ, Lehmann B, Oeschger H, Sigg A, Schwander J, Staf-felbach T, Stauffer B, Suter M, Wölfli W. 1990. Use of ^{10}Be in polar ice to trace the 11-year cycle of solar activity. *Nature* 347(6289):164–6.

Beer J, Siegenthaler U, Bonani G, Finkel RC, Oeschger H, Suter M, Wölfli W. 1988. Information on past so-lar activity and geomagnetism from ^{10}Be in the camp Century ice core. *Nature* 331(6158):675–9.

Broecker WS, Peng T-H. 1986. Carbon cycle: 1985 glacial to interglacial changes in the operation of the global carbon cycle. *Radiocarbon* 28(2A):309–27.

Bronk Ramsey C, Staff RA, Bryant CL, Brock F, Kitagawa H, van der Plicht J, Schlolaut G, Marshall MH, Brauer A, Lamb HF, Payne RL, Tarasov PE, Haraguchi T, Gotanda K, Yonenobu H, Yokoyama Y, Tada R, Nakagawa T. 2012. A complete terrestrial radiocarbon record for 11.2 to 52.8 kyr B.P. *Science* 338(6105):370–4.

Castagnoli G, Lal D. 1980. Solar modulation effects in terrestrial production of carbon-14. *Radiocarbon* 22(2):133–58.

Delaygue G, Bard E. 2011. An Antarctic view of Beryllium-10 and solar activity for the past millennium. *Climate Dynamics* 36(11–12):2201–18.

Elsasser W, Ney EP, Winckler JR. 1956. Cosmic-ray in-tensity and geomagnetism. *Nature* 178(4544):1226– 7.

EPICA Community Members. 2004. Eight glacial cycles from an Antarctic ice core. *Nature* 429(6992):623–8.

EPICA Community Members. 2006. One-to-one coupling of glacial climate variability in Greenland and Antarctica. *Nature* 444(7116):195–8.

Fairbanks RG, Mortlock RA, Chiu TC, Cao L, Kaplan A, Guilderson TP, Fairbanks TW, Bloom AL, Grootes PM, Nadeau M-J. 2005. Radiocarbon calibration curve spanning 0 to 50,000 years BP based on paired $^{230}Th/^{234}U/^{238}U$ and ^{14}C dates on pristine corals. *Quaternary Science Reviews* 24(16–17):1781–96.

Field CV, Schmidt GA, Koch D, Salyk C. 2006. Model-ing production and climate-related impacts on ^{10}Be concentration in ice cores. *Journal of Geophysical Research* 111:D15107, doi:10.1029/2005JD006410.

Finkel RC, Nishiizumi K. 1997. Beryllium 10 concen-trations in the Greenland Ice Sheet Project 2 ice core from 3–40 ka. *Journal of Geophysical Research* 102(C12):26,699–706.

Frank M, Schwarz B, Baumann S, Kubik PW, Suter M, Mangini A. 1997. A 200 kyr record of cosmogen-ic radionuclide production rate and geomagnetic field intensity from ^{10}Be in globally stacked deep-sea sediments. *Earth and Planetary Science Letters* 149(1–4):121–9.

Heikkilä U, Beer J, Feichter J. 2008. Modeling cosmo-genic radionuclides ^{10}Be and ^{7}Be during the Maun-der Minimum using the ECHAM5-HAM General Circulation Model. *Atmospheric Chemistry and Physics* 8:2797–809.

Heikkilä U, Beer J, Feichter J. 2009. Meridional trans-port and deposition of atmospheric ^{10}Be. *Atmospher-ic Chemistry and Physics* 9:515–27.

Hoffmann DL, Beck JW, Richards DA, Smart PL, Sing-arayer JS, Ketchmark T, Hawkesworth CJ. 2010. Towards radiocarbon calibration beyond 28 ka using speleothems from the Bahamas. *Earth and Plane-tary Science Letters* 289(1–2):1–10.

Horiuchi K, Uchida T, Sakamoto Y, Ohta A, Matsuzaki H, Shibata Y, Motoyama H. 2008. Ice core record of ^{10}Be over the past millennium from Dome Fuji, Ant-arctica: a new proxy record of past solar activity and a powerful tool for stratigraphic dating. *Quaternary Geochronology* 3(3):253–61.

Hughen K, Lehman S, Southon J, Overpeck J, Marchal O, Herring C, Turnbull J. 2004. ^{14}C activity and global carbon cycle changes over the past 50,000 years. *Science* 303(5655):202–7.

Hughen K, Southon J, Lehman S, Bertrand C, Turnbull J. 2006. Marine-derived ^{14}C calibration and activi-ty record for the past 50,000 years updated from the Cariaco Basin. *Quaternary Science Reviews* 25(23):3216–27.

Indermühle A, Monnin E, Stauffer B, Stocker TF. 2000. Atmospheric CO_2 concentration from 60 to 20 kyr BP from the Taylor Dome ice core, Antarctica. *Geophysical Research Letters* 27(5):735–8.

Johnsen SJ, Dahl-Jensen D, Gundestrup N, Steffensen

JP, Clausen HB, Miller H, Masson-Delmotte V, Sveinbjörnsdottir AE, White J. 2001. Oxygen isotope and palaeotemperature records from six Green-land ice-core stations: Camp Century, Dye-3, GRIP, GISP2, Renland and NorthGRIP. *Journal of Quater-nary Science* 16(4):299–307.

Kovaltsov GA, Usoskin IG. 2010. A new 3D numerical model of cosmogenic nuclide ^{10}Be production in the atmosphere. *Earth and Planetary Science Letters* 291(1–4):182–8.

Kovaltsov GA, Mishev AL, Usoskin IG. 2012. A new model of cosmogenic production of radiocarbon ^{14}C in the atmosphere. *Earth and Planetary Science Let-ters* 337–338:114–20.

Laj C, Kissel C, Mazaud A, Michel E, Muscheler R, Beer J. 2002. Geomagnetic field intensity, North At-lantic Deep Water circulation and atmospheric Δ^{14}C during the last 50 kyr. *Earth and Planetary Science Letters* 200(1–2):177–90.

Laj C, Kissel C, Beer J. 2004. High resolution global paleointensity stack since 75 kyr (GLOPIS-75) cal-ibrated to absolute values. In: Channell JET, Kent DV, Lowrie W, Meert JG, editors. *Timescales of the Paleomagnetic Field*. Washington, DC: American Geophysical Union. p 255–65.

Lal D, Peters B. 1967. Cosmic ray produced radioac-tivity on the Earth. In: Sittle K, editor. *Handbuch der Physik*. Volume 46/2. Berlin: Springer Verlag. p 551–612.

Lisiecki LE, Lisiecki PA. 2002. Application of dynam-ic programming to the correlation of paleoclimate records. *Paleoceanography* 17:1049, doi:10.1029/ 2001PA000733.

Masarik J, Beer J. 1999. Simulation of particle fluxes and cosmogenic nuclide production in the Earth's atmosphere. *Journal of Geophysical Research* 104(D10):12,099–111.

Masarik J, Beer J. 2009. An updated simulation of particle fluxes and cosmogenic nuclide production in the Earth's atmosphere. *Journal of Geophysical Research* 114:D11103, doi:10.1029/2008JD010557.

Mazaud A, Laj C, Bender M. 1994. A geomagnetic chronology for antarctic ice accumulation. *Geophys-ical Research Letters* 21(5):337–40.

Ménabréaz L, Thouveny N, Bourlès DL, Hamelin B, Demory F. 2011. The Laschamp geomagnetic dipole low expressed as a cosmogenic ^{10}Be atmospheric overproduction at ~41 ka. *Earth and Planetary Sci-ence Letters* 312(3–4):305–17.

Muscheler R, Beer J, Wagner G, Laj C, Kissel C, Raisbeck GM, Yiou F, Kubik PW. 2004. Changes in the carbon cycle during the last deglaciation as indicated by the comparison of ^{10}Be and ^{14}C records. *Earth and Planetary Science Letters* 219(3–4):325–40.

Muscheler R, Beer J, Kubik PW, Synal H-A. 2005. Geomagnetic field intensity during the last 60,000 years based on ^{10}Be and ^{36}Cl from the Summit ice cores and ^{14}C. *Quaternary Science Reviews* 24(16–17):1849–60.

Muscheler R, Kromer B, Björck S, Svensson A, Friedrich M, Kaiser KF, Southon J. 2008. Tree rings and ice cores reveal ^{14}C calibration uncertainties during the Younger Dryas. *Nature Geoscience* 1:263–7.

Nilsson A, Muscheler R, Snowball I, Aldahan A, Possnert G, Augustinus P, Atkin D, Stephens T. 2011. Multi-proxy identification of the Laschamp geomagnetic field excursion in Lake Pupuke, New Zea-land. *Earth and Planetary Science Letters* 311(1– 2):155–64.

Paillard D. 1995. Modèles simplifiés pour l'étude de la variabilité de la circulation thermohaline au cours des cycles glaciaire–interglaciaire [PhD thesis]. Université Paris XI.

Paillard D, Labeyrie L, Yiou P. 1996. Macintosh program performs time-series analysis. *Eos Transactions AGU* 77(39):379.

Raisbeck GM, Yiou F, Fruneau M, Loiseaux JM, Lieuvin M, Ravel JC. 1981. Cosmogenic ^{10}Be/^{7}Be as a probe of atmospheric transport processes. *Geophysical Research Letters* 8(9):1015–8.

Raisbeck GM, Yiou F, Bourles D, Kent DV. 1985. Evidence for an increase in cosmogenic ^{10}Be during a geomagnetic reversal. *Nature* 315(6017):315–7.

Raisbeck GM, Yiou F, Jouzel J, Petit JR. 1990. ^{10}Be and δ^{2}H in polar ice cores as a probe of the solar variability's influence on climate. *Philosophical Transac-tions of the Royal Society of London A* 330:463–70.

Raisbeck GM, Yiou F, Jouzel J, Petit JR, Barkov NI, Bard E. 1992. ^{10}Be deposition at Vostok, Antarctica during the last 50,000 years and its relationship to possible cosmogenic production variations during this period. In: Bard E, Broecker WS, editors. *The Last Deglaciation: Absolute and Radiocarbon Chronologies*. NATO ASI Series I2. Berlin: Springer. p 127–39.

Raisbeck GM, Yiou F, Jouzel J, Stocker TF. 2007. Di-rect north-south synchronization of abrupt climate change record in ice cores using Beryllium 10. *Cli-mate of the Past* 3:541–7.

Reimer PJ, Baillie MGL, Bard E, Bayliss A, Beck JW, Bertrand C, Blackwell PG, Buck CE, Burr GS, Cut-ler KB, Damon PE, Edwards RL, Fairbanks RG, Friedrich M, Guilderson TP, Hughen KA, Kromer B, McCormac FG, Manning S, Bronk Ramsey C, Reimer RW, Remmele S, Southon JR, Stuiver M, Talamo S, Taylor FW, van der Plicht J, Weyhen-meyer CE. 2004. IntCal04 terrestrial radiocarbon age calibration, 0–26 cal kyr BP. *Radiocarbon* 46(3):1029–58.

Reimer PJ, Baillie MGL, Bard E, Bayliss A, Beck JW, Blackwell PG, Bronk Ramsey C, Buck CE, Burr GS, Edwards RL, Friedrich M, Grootes PM, Guilderson TP, Hajdas I, Heaton TJ, Hogg AG, Hughen KA, Kaiser KF, Kromer B, McCormac FG, Manning SW, Reimer RW, Richards DA, Southon JR, Talamo S, Turney CSM, van der Plicht J, Weyhenmeyer CE. 2009. IntCal09 and Marine09 radiocarbon age cali-bration curves, 0–50,000 years cal BP. *Radiocarbon* 51(4):1111–50.

Reimer PJ, Bard E, Bayliss A, Beck JW, Blackwell PG,

Bronk Ramsey C, Buck CE, Cheng H, Edwards RL, Friedrich M, Grootes PM, Guilderson TP, Haflida-son H, Hajdas I, Hatté C, Heaton TJ, Hoffman DL, Hogg AG, Hughen KA, Kaiser KF, Kromer B, Man-ning SW, Niu M, Reimer RW, Richards DA, Scott EM, Southon JR, Staff RA, Turney CSM, van der Plicht J. 2013. IntCal13 and Marine13 radiocarbon age calibration curves 0–50,000 years cal BP. *Radio-carbon* 55(4):1869–87.

Robinson C, Raisbeck GM, Yiou F, Lehman B, Laj C. 1995. The relationship between ^{10}Be and geomagnetic field strength records in central North Atlantic sediments during the last 80 ka. *Earth and Planetary Science Letters* 136(3–4):551–7.

Siegenthaler U, Heimann M, Oeschger H. 1980. ^{14}C variations caused by changes in the global carbon cycle. *Radiocarbon* 22(2):177–91.

Singer BS, Guillou H, Jicha BR, Laj C, Kissel C, Beard BL, Johnson CM. 2009. ^{40}Ar/^{39}Ar, K-Ar and ^{230}Th-^{238}U dating of the Laschamp excursion: a radioiso-topic tie-point for ice core and climate chronology. *Earth and Planetary Science Letters* 286(1–2):80–8.

Svensson A, Andersen KK, Bigler M, Clausen HB, Dahl-Jensen D, Davies SM, Johnsen SJ, Muscheler R, Parrenin F, Rasmussen SO, Röthlisberger R, Seierstad I, Steffensen JP, Vinther BM. 2008. A 60 000 year Greenland stratigraphic ice core chronology. *Climate of the Past* 4:47–57.

Turney CSM, Fifield LK, Hogg AG, Palmer G, Hugh-en K, Baillie MGL, Galbraith R, Ogden J, Lorrey A, Tims SG, Jones RT. 2010. The potential of New Zealand kauri (*Agathis australis*) for testing the syn-chronicity of abrupt climate change during the Last Glacial Interval (60,000–11,700 years ago). *Quater-nary Science Reviews* 29(27–28):3677–82.

Usoskin IG, Alanko-Huotari K, Kovaltsov GA, Mursula K. 2005. Heliospheric modulation of cosmic rays: monthly reconstruction for 1951–2004. *Journal of Geophysical Research* 110:A12108, doi:10.1029/ 2005JA011250.

Wagner G, Masarik J, Beer J, Baumgartner S, Imboden D, Kubik PW, Synal H-A, Suter M. 2000. Reconstruction of the geomagnetic field between 20 and 60 kyr BP from cosmogenic radionuclides in the GRIP ice core. *Nuclear Instruments and Methods in Physics Research B* 172(1–4):597–604.

Wagner G, Beer J, Masarik J, Muscheler R, Kubik PW, Mende W, Laj C, Raisbeck GM, Yiou F. 2001. Presence of the solar de Vries cycle (~205 years) during the last ice age. *Geophysical Research Letters* 28(2):303–6.

Webber WR, Higbie PR. 2003. Production of cosmo-genic Be nuclei in the Earth's atmosphere by cos-mic rays: its dependence on solar modulation and the interstellar cosmic ray spectrum. *Journal of Geophysical Research* 108:1355, doi:10.1029/ 2003JA009863.

Yiou F, Raisbeck GM, Bourles D, Lorius C, Barkov Nl. 1985. ^{10}Be in ice at Vostok Antarctica during the last climatic cycle. *Nature* 316(6029):616–7.

Yiou F, Raisbeck GM, Baumgartner S, Beer J, Hammer C, Johnsen S, Jouzel J, Kubik PW, Lestringuez J, Stiévenard M, Suter M, Yiou P. 1997. Beryllium 10 in the Greenland Ice Core Project ice core at Sum-mit, Greenland. *Journal of Geophysical Research* 102(C12):26,783–94.

4. Note added in proof: When this manuscript was submitted, and accepted, the most recent calibration curve available was IntCal09. In the intervening time period, IntCal13 has been published. We have therefore added this new curve in Figures 7 and S2. The main differences are (i) the amplitude of ^{14}C at the time of the Laschamp event is significantly reduced and is now in better agreement with modeled results, especially those using the KOV calculations; (ii) the slope of the ^{14}C rise at the beginning of the Laschamp event is considerably steeper, and in better agreement with the ^{10}Be-based modeled data. Thus, the improved agreement of the modeled ^{14}C with that based on ^{10}Be suggests that IntCal13 is indeed an improvement over IntCal09 in the time period around the Laschamp event.